Inorganic Chemistry
Cite This: Inorg. Chem. 2019, 58, 2979−2986
Article
pubs.acs.org/IC

Hydrogen Evolution in [NiFe] Hydrogenases: A Case of Heterolytic Approach between Proton and Hydride

Siyao Qiu,[†,‡] Luis Miguel Azofra,[§] Douglas R. Macfarlane,[*,‡,∥] and Chenghua Sun[*,†,⊥]

[†]Science & Technology Innovation Institute, Dongguan University of Technology, Dongguan 523808, China
[‡]School of Chemistry, Faculty of Science, Monash University, Clayton, VIC 3800, Australia
[§]KAUST Catalysis Center (KCC), King Abdullah University of Science and Technology (KAUST), Thuwal 23955-6900, Saudi Arabia
[∥]ARC Centre of Excellence for Electromaterials Science (ACES), School of Chemistry, Faculty of Science, Monash University, Clayton, VIC 3800, Australia
[⊥]Department of Chemistry and Biotechnology, Faculty of Science, Engineering and Technology, Swinburne University of Technology, Hawthorn, VIC 3122, Australia

Supporting Information

ABSTRACT: The mechanism for Hydrogen Evolution Reaction (HER) in [NiFe] hydrogenase enzymes distinguishes them from inorganic catalysts. The first H^+/e^- pair injected to the active site of the hydrogenases transforms into hydride, while the second H^+/e^- pair injection leads to the formation of the H^-/H^+ pair both binding to the active site. The two opposite charged hydrogens heterolytically approach each other in order to form dihydrogen (H_2), which is enhanced by the Coulomb force. Two previously proposed reaction routes for this process have been examined by Conceptual Density Functional Theory (DFT) in this work. One presents better agreement with experimental spectra, while the other is thermodynamically more favorable. Both paths suggest that the approach and the charge transfer between the proton and hydride are motivated by the stabilization of the electronic activity and the electrophilicity of Ni. After the heterolytic approach of the proton and hydride moieties, the two hydrogen atoms attach to the Ni ion and combine homolytically.

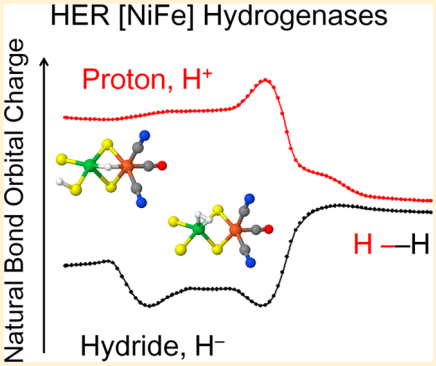

1. INTRODUCTION

Dihydrogen (H_2), as a carbon-free energy carrier, is emerging as a promising future energy alternative.[1] However, the large-scale production of H_2 is limited by the lack of low-cost and highly efficient catalysts, as the existing high-performance catalysts for H_2-production usually involve noble metals, such as platinum.[2] In Nature, hydrogenase enzymes are found in particular organisms and exhibit impressive catalytic properties; more importantly, they are based on earth-abundant elements.[3] Therefore, the understanding of the low overpotential and kinetics barrier of hydrogenases is of special significance.

Hydrogenases can be classified, considering the different metal ions at the active site, into [NiFe], [FeFe], and [Fe] species.[4,5] The [NiFe] hydrogenases catalyze the hydrogen evolution reaction (HER) and the reverse hydrogen cleavage into protons (H^+) and electrons (e^-), but also some particular [NiFe] hydrogenases demonstrate better oxygen tolerance than the [FeFe] kind.[6−8] The active site of [NiFe] hydrogenases consists of a four-membered ring involving nickel, iron, and two bridging sulfurs from cysteine residues. In addition, two terminal cysteine residues connect with Ni via S, while one carbonyl and two cyanide groups ligate with Fe through C.[9]

Typically, HER on most inorganic catalysts mechanistically follows the Volmer−Tafel (V−T) route (Scheme 1).[1,10] In this, two protons combine with two electrons separately on the surface of the catalyst to finally form H_2 homolytically from two adsorbed H atoms. Alternatively, in the Volmer−Heyrovsky (V−H) mechanism, the second proton from the environment directly approaches the first H-adatom to subsequently form H_2. For the [NiFe] hydrogenases, it is accepted that the enzyme catalyzes the H_2 evolution/cleavage heterolytically.[11,12] However, the difference between the H_2

Scheme 1. Mechanisms of HER Following the Volmer−Tafel and Volmer−Heyrovsky Routes

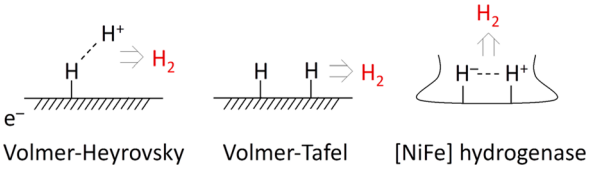

Received: October 4, 2018
Published: February 12, 2019

DOI: 10.1021/acs.inorgchem.8b02812
Inorg. Chem. 2019, 58, 2979−2986

combination mechanism on the [NiFe] hydrogenases and the V−H mechanism on inorganic catalysts is still unclear. In our study, we delve into the mechanistic aspects about how and why the H^- and H^+ moieties, both binding on the active site, heterolytically approach each other in order to form H_2.

To understand the whole HER path in [NiFe] hydrogenases, a general view of the reaction is shown in Scheme 2.[12,13] The injection of the first H^+/e^- pair to the initial state,

Scheme 2. HER Path Followed by [NiFe] Hydrogenases

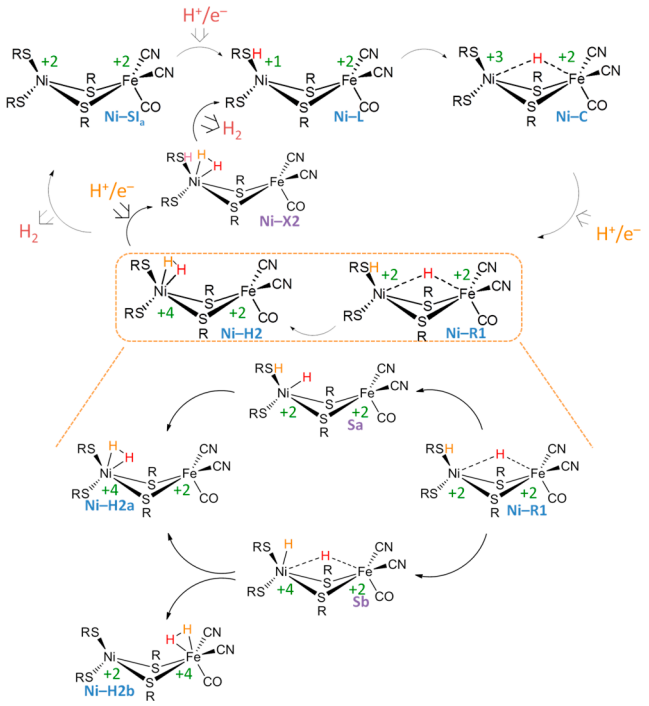

Ni-SIa,[14−19] leads to the **Ni-C** state. In this, the negative hydride is formed between the Ni and Fe centers which leads to (or is promoted by) the conversion of the Ni redox state to Ni^{III}.[20−25] The **Ni-L** state is postulated to connect the **Ni-SIa** and **Ni-C** states, in which the proton that is delivered to the active site first binds to the terminal S atom at the active site, while the electron goes to Ni, altering the redox state of Ni from Ni^{II} to Ni^{I}.[26] Recent DFT investigations carried out by us have proven that two electron transfers occur asynchronously, being motivated by the stabilization of electronic activity and the decrease of the electrophilicity index of Ni.[27] Then, the **Ni-R1** state is generated with the second H^+/e^- pair injection. Similar to what happened with the first H^+/e^- pair, the second proton is added to the terminal S and the electron is injected into Ni, changing the Ni redox state from Ni^{III} to the original Ni^{II}.[28−32] The structure has been confirmed by X-ray crystallography work by Ogata et al.[34] Our previous Fourier transform infrared (FTIR) calculation on the **Ni-R1** state also suggested good agreement to experimental data.[35] Based on these results, this proton is proposed to be transferred to the metal center, generating chemisorbed H_2 through the combination with the hydride on the Ni or Fe ion in the so-called **Ni-H2** state.[15,36,37] According to previous studies, pure functionals show better agreement with the geometry detected by the experiment than hybrid functionals; moreover, they offer better agreement with energy results by CCSD(T) calculations.[38] Computational calculations using pure functionals suggest that the singlet path is thermodynamically more favorable than the triplet path.[12,39−41] For H_2-adsorption, Ni- and Fe-bindings are preferred at low- and high-spin state calculations.[11,15,41] Therefore, it is widely accepted that the H_2 binds to the Ni ion at the active site of [NiFe] hydrogenases.[11,12,41] In previous work by Bruschi et al., two different paths for the proton and hydride combination have been proposed (**Sa** or **Sb**).[11] In addition to the reaction path via **Ni-H2** to **Ni-SI$_a$** state shown in Scheme 2, the other possible path through the **Ni-H2** to **Ni-L** state has also been proposed by Nillson Lill and Siegbahn.[39]

Two other **Ni-R** substates (**Ni-R2** and **Ni-R3**) have been detected by FTIR spectroscopy.[28,33] The **Ni-R2** and **Ni-R3** states were assigned to be the most reduced active states, and they might be different protonation states with the **Ni-R1** state based on FTIR experiment; however, these two structures are not clearly determined.[28] Therefore, we proposed that the two **Ni-R** substates might be the intermediate states for the following H_2 generation from the **Ni-R1** state. This work focused on the studies of these two states and aimed to deliver a detailed catalytic mechanism from **Ni-R1** to **Ni-H2**. The key challenge is to identify the structures for **Ni-R2** and **Ni-R3**, which are expected to not only agree with the FTIR experiments but also lead to reasonable HER paths in terms of energy.

2. COMPUTATIONAL DETAILS

Calculations of the geometries and energies for the **Ni-R1** to **Ni-H2** step by [NiFe] hydrogenases have been performed through Density Functional Theory (DFT) via the BP86 functional, with two-layered basis sets:[43−45] a higher level basis set Def2TZVPP has been applied for the core part of the active site, including the two metal ions, the three diatomic inorganic ligands, and the four binding sulfurs; correspondingly, a lower level basis set Def2SVP has been used for the remaining portion of the models.[46] Also, functional M06 with the same basis sets has been applied to the Small model calculation, and the results are shown in the Supporting Information (SI). Accordingly, the geometry optimizations have been done to locate the minima, and the transition states have been searched through the Synchronous Transit-Guided Quasi-Newton (STQN) method (QST3).[47] To confirm the nature of the stationary points and obtain the free energy changes, in both cases, frequency calculations have been conducted. Also, the Intrinsic Reaction Coordinate (IRC) method was used for the exploration of the intermediate structures between minima and transition states, with the reaction coordinate (ξ) expressed in mass-weighted internal coordinates.[48] The IRC calculations have been employed using step sizes equal to 0.05 bohr. The dispersion interactions have been corrected by using the Grimme's D3 damping function.[49] All calculations were carried out by Gaussian09 (revision D.01).[50] The orbital and charge parameters were studied by Natural Bond Orbital (NBO) analysis with the NBO 6.0 program.[51,52]

The models were built based on the X-ray crystallographic data provided by Higuchi et al. for the reduced *Desulfovibrio vulgaris* "Miyazaki F" [NiFe] hydrogenase from organism (PDB code 1H2R).[14] Two models have been used in this work. The "Small" model consists of the metal ions, inorganic ligands and four directly ligated Cys81, Cys84, Cys546, and Cys549 residues, and the "Large" model comprises the "Small" model plus the truncated first amino acids shell around (Glu34, Val83, His88, Asp123, Ala477, Pro478, Arg479,

DOI: 10.1021/acs.inorgchem.8b02812
Inorg. Chem. 2019, 58, 2979−2986

Leu482, Val500, Pro501, Ser502, Ala548, and Ile547). Only the "Small" model has been used for the IRC calculation. The distal carbon atoms have been frozen during the optimization to imitate the real geometry in protein environment. In order to mimic the experimental geometry of the protein environment, a set of atoms have been frozen during optimization. In the Small model, the distal carbon atoms and one of the hydrogen atoms connected to the distal carbon of the four cysteine residues are kept frozen. The atoms that have been constrained in the "Large" model are shown in Figure S3.

3. RESULTS AND DISCUSSION

In the present work, our efforts are focused on unraveling the mechanistic aspects involving the hydride−proton combination (**Ni-R** to **Ni-H2** steps) leading to H_2 in [NiFe] hydrogenases. To understand this process, the structure of the three subforms of the **Ni-R** state and how they are involved in the catalytic pathway should be investigated first. We have calculated the five different possible structures based on Scheme 2 that might participate into the hydride−proton combination process (see Figure 1). Our calculation on the five structures demonstrated that the CO vibration of the five states are 1898, 1867, 1905, 1891, and 1941 cm^{-1} for the **Ni-R1**, **Sa**, **Sb**, **Ni-H2a**, and **Ni-H2b** states, respectively. Also, the most reduced state, **Ni-X2**, among the reaction cycle in Scheme 2 has also been calculated, which shows a vibrational frequency of 1879 cm^{-1} for the CO ligand.

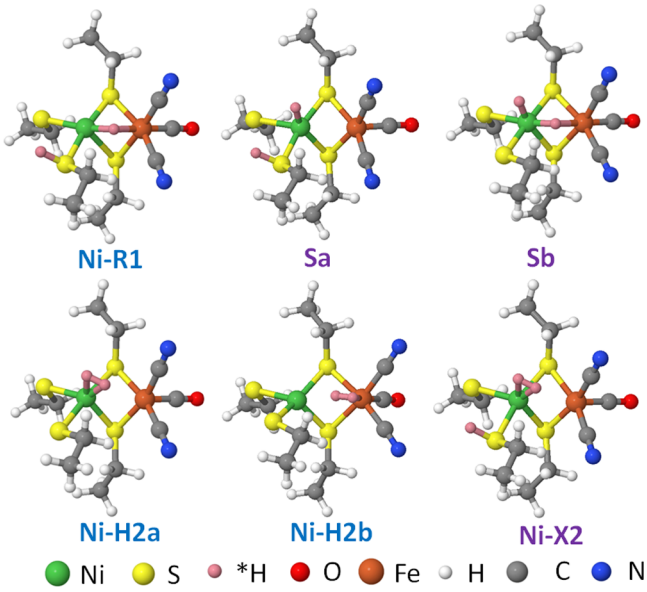

Figure 1. Molecular modeling of the possible structures participated in the hydride-proton combination process by [NiFe] hydrogenases. Hydrogen atoms participating in the HER pathway are highlighted in pink.

The CO vibrational frequencies for the **Ni-R1**, **Ni-R2**, and **Ni-R3** states are 1948, 1932, and 1919 cm^{-1}, as listed in Table 1. Based on early studies of the FTIR spectroscopy with the Small model, our calculation of the CO ligand vibration between the experimental shows a uniformed difference around 50 cm^{-1} as determined by the computational setting.[35] The **Sa** state matches with the **Ni-R3** FTIR data. Moreover, we have calculated the **Sa** state by the Small model with a protonated Glu34, and the FTIR result still shows good agreement (−48 cm^{-1}) with the **Ni-R3** experimental vibration (see SI). As for the **Ni-R2** state, the **Ni-X2** state in Scheme 2 fits well with the **Ni-R2** data. Furthermore, we have also tested another eight possible structures proposed by early studies (see SI),[53−55] and none of the remainder matches with the **Ni-R2** or **Ni-R3** FTIR data. Therefore, we could relate the **Ni-X2** with **Ni-R2** state appeared in the FTIR spectrum and link the **Sa** with the **Ni-R3**.

The difference of the CO vibration between the calculation states (**Ni-X2** and **Sa**) and the FTIR experiment states (**Ni-R2** and **Ni-R3**) are shown in Table 1. The second column is the calculated data by the Small model, the fourth column is the FTIR result of the Large model, and the sixth one is the FTIR calculation result by previous work.[30,56] The accordance of FTIR calculation of the **Ni-X2** state with that of the **Ni-R2** state further supports the H_2 binding to Ni, rather than Fe.

The discrepancies between the computational frequencies and experimental FTIR data are around 25 cm^{-1} in early studies.[30,56] The CO vibrational frequencies associated with various models with different sizes have been calculated by Kampa et al., suggesting that the Large model with the second coordination sphere shows a smaller discrepancy with experimental data compared with the Small one.[56] Therefore, we have calculated the FTIR by the "Large" model, and a deviation around 26 cm^{-1} could be found between our calculation with the experimental data.

Based on the structures proposed by the FTIR calculations, we have investigated the reaction pathway for the proton−hydride combination, which is the step from **Ni-R1** to **Ni-H2a**. Our findings demonstrate that (i) the reaction occurs through two steps with the location of an intermediate state;[11] (ii) the

Table 1. FTIR Experiment[5] and Calculation Data[30,35,37,56] for Different States in [NiFe] hydrogenases, Indicating the Difference between the Experimental and Calculation Results (cm^{-1})[a]

states	ΔCO exp	ΔCO cal Small	Δ	ΔCN cal Large	Δ	ΔCO cal pre	Δ
Ni-A	1956	1905	−51	1929	−27		
Ni-B	1955	1903	−52	1928	−27	1931[a]	−24
Ni-SI_a	1943	1885	−58	1907	−36	1913[a]	−30
Ni-C	1961	1903	−58	1934	−27	1936,[a] 1941[b]	−45
Ni-R1	1948	1898	−50	1928	−20	1923[a]	−25
Ni-R2/Ni-X2	1932	1879	−53	1906	−26		
Ni-R3/Sa	1919	1867	−52	1901	−18		
Sb	1919	1905	−14	1935	16		
Ni-H2a		1891		1919		1926[a]	
Ni-H2b		1941		1963		1962[a]	

[a]The calculation data by ref 30. [b]The calculation data by ref 56.

DOI: 10.1021/acs.inorgchem.8b02812
Inorg. Chem. 2019, 58, 2979−2986

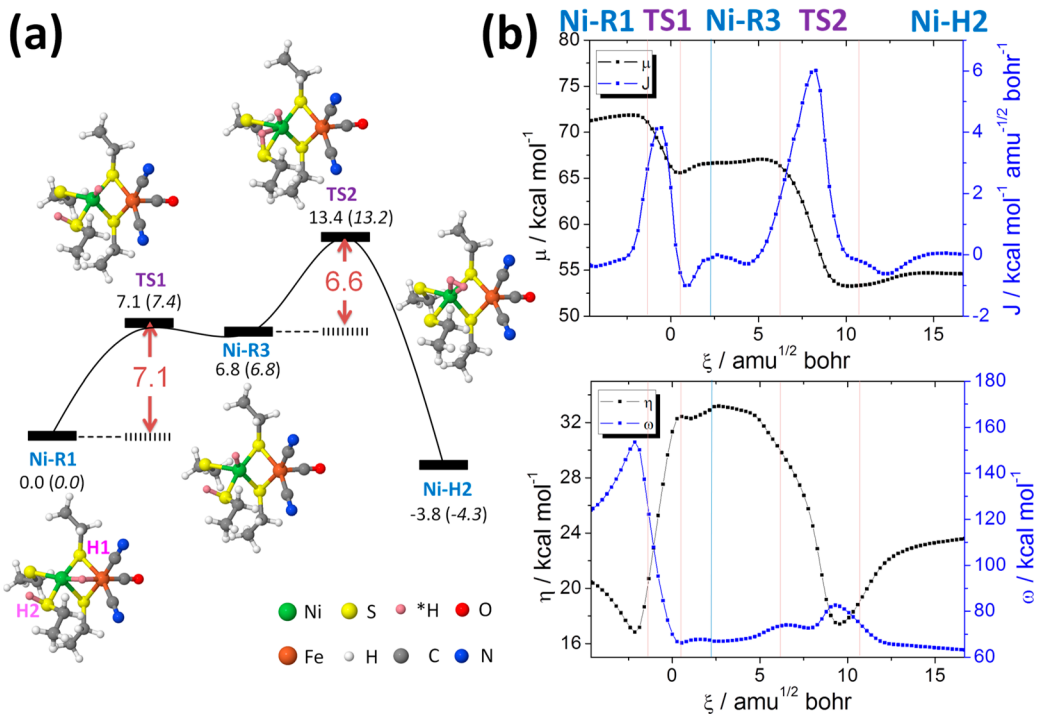

Figure 2. (a) Enthalpy diagram (Gibbs free energies, rt, in parentheses), kcal mol^{-1}, and optimized structures for the **Ni-R1** to **Ni-R2** via **Ni-R3**/**Sa** path of HER by [NiFe] hydrogenase. Note: reactive H atoms are highlighted in pink. (b) (Top) electronic chemical potential, in kcal mol^{-1}, and reaction electronic flux, in kcal mol^{-1} amu$^{-1/2}$ bohr^{-1}, profiles along the reaction pathway; (bottom) total hardness and electrophilicity, in kcal mol^{-1}, profiles. Note: red lines separate the different regions through the intrinsic reaction coordinate.

reaction is enhanced by Coulombic interactions and motivated by the stabilization of electronic activity and electrophilicity of Ni; and (iii) such a process goes through the heterolytic approach of the H^-/H^+ pair.

As indicated in Figure 2a, the reaction mechanism for the hydride−proton evolution into H_2 by [NiFe] hydrogenase presents two steps in our DFT calculations. In the first, the bridging hydride attached to the metal center in the **Ni-R1** state migrates from the bridging binding between Ni and Fe to the terminal binding on the NiII moiety in an endothermic (ΔH_R = 6.8 kcal mol^{-1}), endergonic (ΔG_R = 6.8 kcal mol^{-1}) process, demanding 7.1 kcal mol^{-1} as the activation enthalpy (ΔG_{act} = 7.4 kcal mol^{-1}).

In the following step, the enthalpy change from **Ni-R3** to **Ni-H2** is exothermic, −10.6 kcal mol^{-1} (also spontaneous, ΔG_R = −11.1 kcal mol^{-1}) with an enthalpy barrier of 6.6 kcal mol^{-1} (ΔG_{act} = 6.4 kcal mol^{-1}). In this stage, the proton and hydride approach each other and later two transformed hydrogens combine to form H_2.

As shown in Figure 2b, from **Ni-R3** to **Ni-H2**, the decrement for both electronic chemical potential and reaction electronic flux (REF) becomes significantly positive, suggesting that the electron transfer in the hydride−proton approach that takes place is driven by the stabilization of the electronic rearrangement. Detailed explanations of the parameters are listed in the SI.

The analysis of the total hardness and electrophilicity profiles (Figure 2b, bottom) offers an interesting perspective in understanding how these reactivity descriptors are related to the chemical events taking place. Pearson stated his maximum hardness principle (MHP), noting that "a chemical system at a given temperature will evolve to a configuration of maximum absolute hardness, η".[57] This general behavior is directly related to the minimum electrophilicity principle (MEP), since a chemical system will therefore evolve to a configuration of minimum absolute electrophilicity, ω. Thus, the larger the η, the smaller the ω, and vice versa.

Analyzing them by steps, it is observed that the system evolves through a maximum hardness−minimum electrophilicity pathway along the **TS1** intrinsic reaction coordinate region. Although a decrease and an increase of η and ω respectively are observed once the **Ni-H2** minimum is reached, together with the compliance of MH and ME principles being seen; i.e., this process is driven by a positive and negative balance of η and ω equal to 3.1 and −60.8 kcal mol^{-1}, respectively.

We have also searched for other evidence of this. Previously, our analysis had been focused on the interpretation of the information provided by global Conceptual DFT (CDFT) descriptors. Notwithstanding, chemical reactivity resides in local moieties/atoms exhibiting specific functionalities. In this sense, Figure 3 shows the evolution of the local electrophilicity indexes and the NBO charges of the S, Ni, and Fe atoms that are involved in the hydride−proton → H_2 process. Results show differentiated behaviors not only among them but also along the reaction coordinate as follows:

(i) During the **TS1** region, ω(Ni) decreases. The Ni electrophilicity is stabilized as the hydride transformed from bridging binding between Ni and Fe to the terminal binding to Ni. Since the hydride is a negatively charged moiety, the approach of the hydride to the positively charged Ni is an electrophile−nucleophile neutralization. Similarly, with the hydride moving away, the negatively charged Fe becomes less electrophilic, contributing to the slight decrease of ω(Fe).

DOI: 10.1021/acs.inorgchem.8b02812
Inorg. Chem. 2019, 58, 2979−2986

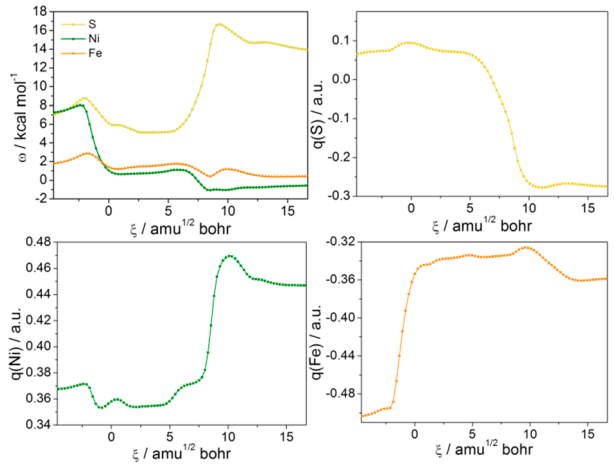

Figure 3. Local electrophilicity index, kcal mol^{-1}, and NBO charge, a.u., profiles for S, Ni, and Fe reactive atoms.

(ii) As for the proton and hydride combination process (**TS2** region), ω(S) increases rapidly with the proton moving away from the S atom, and ω(Ni) decreases with the proton−hydride approaching. During the two steps, ω(Fe) remains practically stable compared with Ni and S. This is in accord with what we have previously observed in the proton conversion into hydride (**Ni-L** to **Ni−C** stage): "the evolution of ω(Fe) along the reaction coordinate illustrates the minor role of this atom as an electrophilic centre".[27]

More importantly, the NBO charge evolution of the H1 (hydride) and H2 (proton) atoms in Figure 4 demonstrate

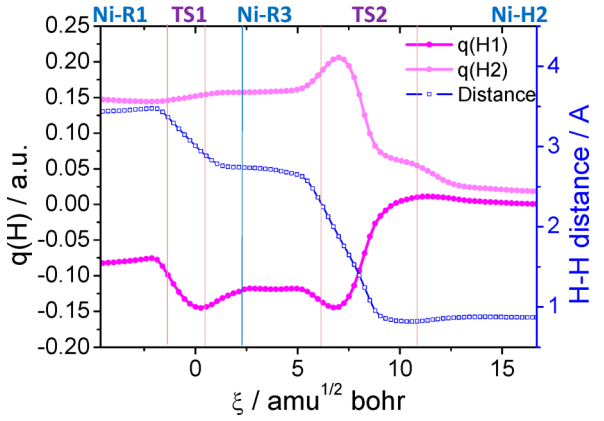

Figure 4. NBO charge, a.u., profile for hydride/H1 (bold pink) and proton/H2 (soft pink), and H1−H2 distance profile, Å. Note: red lines separate the different regions through the intrinsic reaction coordinate.

that once **TS2** is reached, an increase of q(H1) (losing electrons) is directly complemented by a decrease of q(H2) (gaining electrons); i.e., the heterolytic proton hydride approach is demonstrated to be catalyzed by [NiFe] hydrogenase through hydride oxidation−proton reduction being motivated by Coulomb forces. Finally, during **TS2** and up to **Ni-H2**, the approach of the two hydrogens leads to charges being q(H1) ≈ q(H2) ≈ 0, as indication of the H_2 formation.

In the V−H mechanism, the second proton binds directly to the existing hydrogen atom on the catalyst, while, in the [NiFe] hydrogenases system, the second proton binds to the Ni atom before combining with the hydride and the electron transfer between proton and hydride leads to the homolytic hydrogen combination in the **Ni-H2** region. Therefore, the **Ni-H2** stage shows a hydrogen combination mechanism more close to the V−T route. However, the **Ni-R3** to **Ni-H2** process is a heterolytic proton−hydride approach. Thus, the overall proton−hydride combination in the [NiFe] hydrogenases has a different mechanism with both the V−T and V−H routes, which is also supported by the M06 functional calculation (see SI).

It is worth mentioning that the V−T mechanism HER is energetically favorable in most of the inorganic materials compared to the V−H mechanism. Also, the Coulombic interaction between the two hydrogen atoms in the heterolytic V−H mechanism could reduce the energy for the approach. Additionally, the [NiFe] hydrogenase seems to combine the two mechanisms in the inorganic catalysts.

The previous work by Bruschi et al. proposed that the proton−hydride combination path through the **Sb** state is more thermodynamically favorable than the path via the **Sa** state.[11] Dong et al. further supported the small activation barrier via the **Sb** state.[42] Therefore, we have also studied this path by Conceptual DFT calculation (see Figure 5).

From the **Ni-R1** to **Sb** state, the energy barrier of activation is 2.5 kcal/mol, and the reaction energy of this stage is −3.5 kcal/mol. During the stage, the proton steadily moves from S to Ni. The proton in **TS1** is still around the binding S, with a 1.39 Å distance to S and 2.15 Å to Ni. Therefore, the activation energy for the **TS1** is mainly to propel the proton away from the S. The free energy change between the **Sb** and **Ni-H2** state is −0.7 kcal/mol, with a barrier of 0.8 kcal/mol. The two hydrogen atoms combine with each other to form a dihydrogen molecule at this stage.

Similar to the reaction path through **Ni-R3**/**Sa** state, the electronic chemical potential in Figure 5b (left top) shows an apparent decrease during the proton−hydride approach step (**Ni-R1** to **Sb**). Also, the electrophilicity of Ni decreases with the proton approach during the **Ni-R1** to **Sb** step (Figure 5b, right top).

Moreover, the NBO charge change shown in Figure 5b (right bottom) reflects the charge transfer from hydride to proton during the **Ni-R1** to **Sb** step. During the combination step (**Sb** to **Ni-R2**), two hydrogen atoms show charges q(H1) ≈ q(H2) ≈ 0, indicating the homolytic H_2 formation during the step. Therefore, similar conclusions could be drawn from the calculation along the **Ni-R1**, **Sb** to **Ni-H2** path.

The calculations on the two paths for the proton−hydride formation by the "Large" model have also been conducted. The existence of the protein environment reduces thermodynamic reaction energy as well as the activation barrier for each step, while the structures and the trend of the energy profile are very similar to those of the "Small" model. The result agrees with the work by Bruschi and Dong,[11,42] which preferred the **Sb** route than the **Sa** route in terms of reaction energy changes. As there might be some other states we have not fully considered that also fit with the FTIR data, also the high energy barrier from **Ni-H2** to **Sa** suggests little population of the **Sa** state. Therefore, **Sa** could hardly be observed in the FTIR experiment, and thus we also prefer the route via the **Sb** state. Our previous work showed different reaction energies for the **Ni-R** to **Ni-H2** step,[37,58] which is due to a different **Ni-R** structure we proposed with the **Ni-R1** state (see SI). The

DOI: 10.1021/acs.inorgchem.8b02812
Inorg. Chem. 2019, 58, 2979−2986

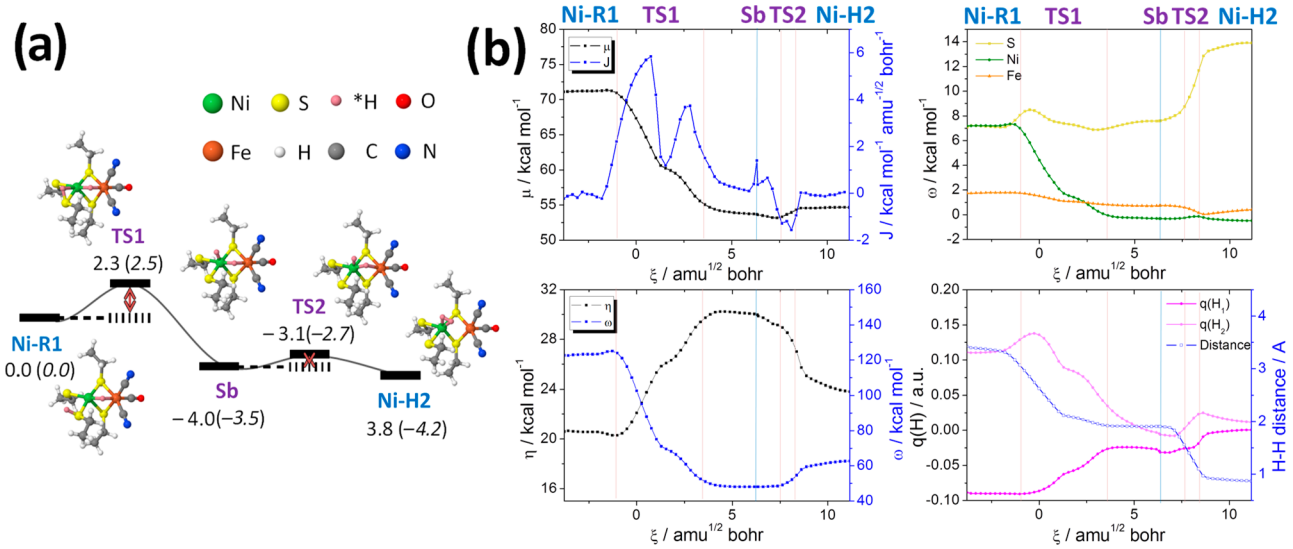

Figure 5. (a) Enthalpy diagram (Gibbs free energies, rt, in parentheses), kcal mol^{-1}, and optimized structures for the **Ni-R1** to **Ni-R2** path via **Sb** state of HER by [NiFe] hydrogenase. (b) (Left top) Electronic chemical potential, in kcal mol^{-1}, and reaction electronic flux, in kcal mol^{-1} amu$^{-1/2}$ bohr^{-1}, profiles along the reaction pathway; (left bottom) total hardness and electrophilicity, in kcal mol^{-1}, profiles; (right top) local electrophilicity index, kcal mol^{-1}; (right bottom) NBO charge, a.u., profile for hydride/H1 (bold pink) and proton/H2 (soft pink), and H1−H2 distance profile.

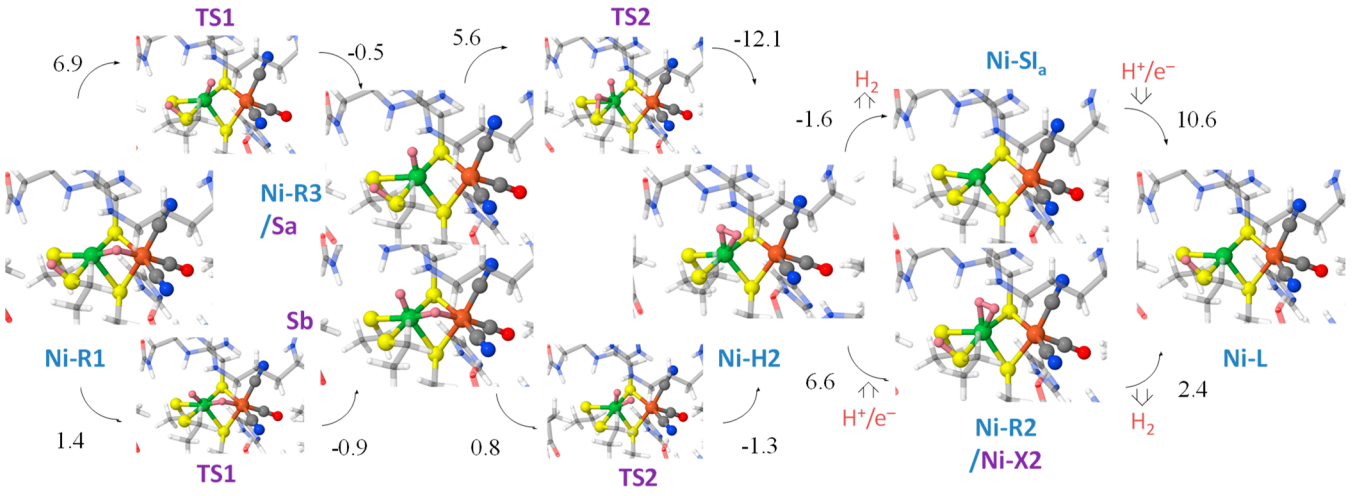

Figure 6. Structures and Gibbs free energy diagram for the **Ni-R1** to **Ni-R2** reaction via two different paths by the "Large" model, in kcal mol^{-1}.

existence or absence of this different **Ni-R** structure during the reaction on [NiFe] hydrogenases would not affect the proton−hydride combination process; consequently, it has not been mentioned in the text.

Furthermore, the "Large" model calculation suggests the reaction via **Ni-X2** requires 6.6 kcal/mol for the following H^+/e^- injection, which is less than the energy required for the H^+/e^- injection step through the **Ni-SI$_a$** path (Figure 6).

Moreover, we have compared the turnover rate of the NiFe hydrogenase with our results.[59] According to the Arrhenius equation and transition state theory, the rate constant $k_{cat.}$ could be expressed as $k_{cat.} = 1/h \cdot k_B T \cdot e^{(-E_a/RT)}$. The rate is around 760 s^{-1} at 303 K. Therefore, the maximum activation barrier for the H_2 reduction on NiFe hydrogenases would be 13.7 kcal/mol. Therefore, the activation energy, no matter from which path, has to be smaller than 13.7 kcal/mol.

4. SUMMARY AND CONCLUSIONS

In summary, the possible structures for the **Ni-R2** and **Ni-R3** states during the catalytic cycle of [NiFe] hydrogenases have been discussed in this work. Also, two possible pathways for H_2 evolution from a proton and hydride by [NiFe] hydrogenases have been studied by Conceptual DFT in this work. The path via **Sa** state presents excellent agreement with the FTIR experimental data, and the path through the **Sb** state exhibits a smaller reaction energy requirement. Both paths follow the maximum hardness−minimum electrophilicity mechanism and consist of the heterolytic proton hydride approach (V−H mechanism), accompanied by the electron transfer from hydride to proton, and two hydrogen atoms attached to the Ni center homolytically combining (V−T mechanism) to form H_2. Therefore, the proton−hydride combination in [NiFe] hydrogenases is not a pure V−T or V−H mechanism for the HER process. Moreover, the heterolytic approach of proton and hydride in these two paths are both driven by the Coulombic interaction and stabilized by a decrease of the electronic activity and the electrophilicity of Ni.

DOI: 10.1021/acs.inorgchem.8b02812
Inorg. Chem. 2019, 58, 2979−2986

■ ASSOCIATED CONTENT

Supporting Information

The Supporting Information is available free of charge on the ACS Publications website at DOI: 10.1021/acs.inorgchem.8b02812.

Theoretical framework, hybrid functional calculations, large model calculation, polarizable continuum model, basis set test, high-spin calculation, other possible states calculation, Cartesian coordinates for all models (PDF)

■ AUTHOR INFORMATION

Corresponding Authors

*Tel: (+61) 3 9902 9916. Fax: (+61) 3 9905 4597. E-mail: Chenghuasun@swin.edu.au (C.S.).

*Tel: (+61) 3 9905 4540. Fax: (+61) 3 9905 4597. E-mail: Douglas.MacFarlane@monash.edu (D.R.M.).

ORCID

Douglas R. Macfarlane: 0000-0001-5963-9659

Chenghua Sun: 0000-0001-7654-669X

Notes

The authors declare no competing financial interest.

■ ACKNOWLEDGMENTS

The authors acknowledge the financial support from Australian Research Council (ARC), King Abdullah University of Science and Technology and High-level Talents Project of Dongguan University of Technology (Grant Number KCY-KYQD2017017), and Guangdong Innovation Research Team for Higher Education (2017KCXTD030). Gratitude is also due to the National Computational Infrastructure (NCI), which is supported by the Australian Government, and the KAUST Supercomputing Laboratory, using the supercomputer Shaheen II, for providing the computational resources.

■ REFERENCES

(1) He, T.; Gao, G.; Kou, L.; Will, G.; Du, A. Endohedral metallofullerenes (M@C60) as efficient catalysts for highly active hydrogen evolution reaction. *J. Catal.* **2017**, *354*, 231.

(2) Nørskov, J. K.; Bligaard, T.; Logadottir, A.; Kitchin, J. R.; Chen, J. G.; Pandelov, S.; Stimming, U. Trends in the Exchange Current for Hydrogen Evolution. *J. Electrochem. Soc.* **2005**, *152*, J23.

(3) Madden, C.; Vaughn, M. D.; Díez-Pérez, I.; Brown, K. A.; King, P. W.; Gust, D.; Moore, A. L.; Moore, T. A. Catalytic turnover of [FeFe]-hydrogenase based on single-molecule imaging. *J. Am. Chem. Soc.* **2012**, *134*, 1577.

(4) Vignais, P. M.; Billoud, B. Occurrence, Classification, and Biological Function of Hydrogenases: An Overview. *Chem. Rev.* **2007**, *107*, 4206.

(5) Lubitz, W.; Ogata, H.; Rudiger, O.; Reijerse, E. Hydrogenases. *Chem. Rev.* **2014**, *114*, 4081.

(6) Burgdorf, T.; Lenz, O.; Buhrke, T.; van der Linden, E.; Jones, A. K.; Albracht, S. P. J.; Friedrich, B. [NiFe]-hydrogenases of Ralstonia eutropha H16: modular enzymes for oxygen-tolerant biological hydrogen oxidation. *J. Mol. Microbiol. Biotechnol.* **2006**, *10*, 181.

(7) Tard, C.; Pickett, C. J. Structural and Functional Analogues of the Active Sites of the [Fe]-, [NiFe]-, and [FeFe]-Hydrogenases. *Chem. Rev.* **2009**, *109*, 2245.

(8) Fontecilla-Camps, J. C.; Volbeda, A.; Cavazza, C.; Nicolet, Y. Structure/Function Relationships of [NiFe]- and [FeFe]-Hydrogenases. *Chem. Rev.* **2007**, *107*, 4273.

(9) Garcin, E.; Vernede, X.; Hatchikian, E. C.; Volbeda, A.; Frey, M.; Fontecilla-Camps, J. C. The crystal structure of a reduced [NiFeSe] hydrogenase provides an image of the activated catalytic center. *Structure* **1999**, *7*, 557.

(10) Skúlason, E.; Tripkovic, V.; Björketun, M. E.; Gudmundsdóttir, S.; Karlberg, G.; Rossmeisl, J.; Bligaard, T.; Jónsson, H.; Nørskov, J. K. Modeling the Electrochemical Hydrogen Oxidation and Evolution Reactions on the Basis of Density Functional Theory Calculations. *J. Phys. Chem. C* **2010**, *114*, 18182.

(11) Bruschi, M.; Tiberti, M.; Guerra, A.; De Gioia, L. Disclosure of key stereoelectronic factors for efficient H2 binding and cleavage in the active site of [NiFe]-hydrogenases. *J. Am. Chem. Soc.* **2014**, *136*, 1803.

(12) Siegbahn, P. E. M.; Tye, J. W.; Hall, M. B. Computational Studies of [NiFe] and [FeFe] Hydrogenases. *Chem. Rev.* **2007**, *107*, 4414.

(13) Siegbahn, P. E. M. Proton and Electron Transfers in [NiFe] Hydrogenase. *Adv. Inorg. Chem.* **2004**, *56*, 101.

(14) Higuchi, Y.; Ogata, H.; Miki, K.; Yasuoka, N.; Yagi, T. Removal of the bridging ligand atom at the Ni-Fe active site of [NiFe] hydrogenase upon reduction with H2, as revealed by X-ray structure analysis at 1.4 A resolution. *Structure* **1999**, *7*, 549.

(15) Wu, H.; Hall, M. B. Density functional theory on the larger active site models for [NiFe] hydrogenases: Two-state reactivity? *C. R. Chim.* **2008**, *11*, 790.

(16) Volbeda, A.; Fontecilla-Camps, J. C. The active site and catalytic mechanism of NiFe hydrogenases. *Dalton Trans.* **2003**, 4030.

(17) Kurkin, S.; George, S. J.; Thorneley, R. N. F.; Albracht, S. P. Relativistic DFT calculation of the reaction cycle intermediates of [NiFe] hydrogenase: a contribution to understanding the enzymatic mechanism. *Biochemistry* **2004**, *43*, 6820.

(18) Legall, J.; Dervartanian, D. V.; Spilker, E.; Lee, J.-P.; Peck, H. D. Evidence for the involvement of non-heme iron in the active site of hydrogenase from Desulfovibrio vulgaris. *Biochim. Biophys. Acta, Bioenerg.* **1971**, *234*, 525.

(19) Bleijlevens, B.; van Broekhuizen, F. A.; De Lacey, A. L.; Roseboom, W.; Fernandez, V. M.; Albracht, S. P. J. The activation of the [NiFe]-hydrogenase from Allochromatium vinosum. An infrared spectro-electrochemical study. *JBIC, J. Biol. Inorg. Chem.* **2004**, *9*, 743.

(20) Chapman, A.; Cammack, R.; Hatchikian, C. E.; McCracken, J.; Peisach, J. A pulsed EPR study of redox-dependent hyperfine interactions for the nickel centre of Desulfovibrio gigas hydrogenase. *FEBS Lett.* **1988**, *242*, 134.

(21) Kruger, H. J.; Holm, R. H. Stabilization of trivalent nickel in tetragonal NiS4N2 and NiN6 environments: synthesis, structures, redox potentials and observations related to [NiFe]-hydrogenases. *J. Am. Chem. Soc.* **1990**, *112*, 2955.

(22) Krueger, H. J.; Holm, R. H. Chemical and electrochemical reactivity of nickel(II,I) thiolate complexes: examples of ligand-based oxidation and metal-centered oxidative addition. *Inorg. Chem.* **1989**, *28*, 1148.

(23) Foerster, S.; Stein, M.; Brecht, M.; Ogata, H.; Higuchi, Y.; Lubitz, W. Single Crystal EPR Studies of the Reduced Active Site of [NiFe] Hydrogenase from Desulfovibrio vulgaris Miyazaki F. *J. Am. Chem. Soc.* **2003**, *125*, 83.

(24) Brecht, M.; van Gastel, M.; Buhrke, T.; Friedrich, B.; Lubitz, W. Direct Detection of a Hydrogen Ligand in the [NiFe] Center of the Regulatory H2-Sensing Hydrogenase from Ralstonia eutropha in Its Reduced State by HYSCORE and ENDOR Spectroscopy. *J. Am. Chem. Soc.* **2003**, *125*, 13075.

(25) Pardo, A.; De Lacey, A.; Fernández, V.; Fan, H.-J.; Fan, Y.; Hall, M. Density functional study of the catalytic cycle of nickel−iron [NiFe] hydrogenases and the involvement of high-spin nickel(II). *JBIC, J. Biol. Inorg. Chem.* **2006**, *11*, 286.

(26) Stein, M.; Lubitz, W. The electronic structure of the catalytic intermediate Ni-C in [NiFe] and [NiFeSe] hydrogenases. *Phys. Chem. Chem. Phys.* **2001**, *3*, 5115.

(27) Qiu, S.; Azofra, L. M.; MacFarlane, D. R.; Sun, C. Why is a proton transformed into a hydride by [NiFe] hydrogenases? An intrinsic reactivity analysis based on conceptual DFT. *Phys. Chem. Chem. Phys.* **2016**, *18*, 15369.

DOI: 10.1021/acs.inorgchem.8b02812
Inorg. Chem. 2019, 58, 2979−2986

(28) Fichtner, C.; Laurich, C.; Bothe, E.; Lubitz, W. Spectroelectrochemical Characterization of the [NiFe] Hydrogenase of Desulfovibrio vulgaris Miyazaki F. *Biochemistry* **2006**, *45*, 9706.
(29) De Lacey, A. L.; Fernández, V. M.; Rousset, M.; Cammack, R. Activation and Inactivation of Hydrogenase Function and the Catalytic Cycle: Spectroelectrochemical Studies. *Chem. Rev.* **2007**, *107*, 4304.
(30) Kramer, T.; Kampa, M.; Lubitz, W.; van Gastel, M.; Neese, F. Theoretical spectroscopy of the Ni(II) intermediate states in the catalytic cycle and the activation of [NiFe] hydrogenases. *ChemBioChem* **2013**, *14*, 1898.
(31) George, S. J.; Kurkin, S.; Thorneley, R. N. F.; Albracht, S. P. J. Reactions of H2, CO, and O2 with Active [NiFe]-Hydrogenase from Allochromatium vinosum. A Stopped-Flow Infrared Study. *Biochemistry* **2004**, *43*, 6808.
(32) Linford, M. R.; Fenter, P.; Eisenberger, P. M.; Chidsey, C. E. D. Alkyl Monolayers on Silicon Prepared from 1-Alkenes and Hydrogen-Terminated Silicon. *J. Am. Chem. Soc.* **1995**, *117*, 3145.
(33) De Lacey, A. L.; Pardo, A.; Fernandez, V. M.; Dementin, S.; Adryanczyk-Perrier, G.; Hatchikian, E. C.; Rousset, M. FTIR spectroelectrochemical study of the activation and inactivation processes of [NiFe] hydrogenases: effects of solvent isotope replacement and site-directed mutagenesis. *JBIC, J. Biol. Inorg. Chem.* **2004**, *9*, 636.
(34) Ogata, H.; Nishikawa, K.; Lubitz, W. Hydrogens detected by subatomic resolution protein crystallography in a [NiFe] hydrogenase. *Nature* **2015**, *520*, 571.
(35) Qiu, S.; Olsen, S.; MacFarlane, D. R.; Sun, C. Hydrogen bonding effect between active site and protein environment on catalysis performance in H2-producing [NiFe] hydrogenases. *Phys. Chem. Chem. Phys.* **2018**, *20*, 23528.
(36) Keith, J. M.; Hall, M. B. Potential hydrogen bottleneck in nickel-iron hydrogenase. *Inorg. Chem.* **2010**, *49*, 6378.
(37) Qiu, S.; Azofra, L. M.; MacFarlane, D. R.; Sun, C. Unraveling the Role of Ligands in the Hydrogen Evolution Mechanism Catalyzed by [NiFe] Hydrogenases. *ACS Catal.* **2016**, *6*, 5541.
(38) Delcey, M. G.; Pierloot, K.; Phung, Q. M.; Vancoillie, S.; Lindh, R.; Ryde, U. Accurate calculations of geometries and singlet-triplet energy differences for active-site models of [NiFe] hydrogenase. *Phys. Chem. Chem. Phys.* **2014**, *16*, 7927.
(39) Lill, S. O. N.; Siegbahn, P. E. M. An Autocatalytic Mechanism for NiFe-Hydrogenase: Reduction to Ni(I) Followed by Oxidative Addition. *Biochemistry* **2009**, *48*, 1056.
(40) Bruschi, M.; De Gioia, L.; Zampella, G.; Reiher, M.; Fantucci, P.; Stein, M. A Theoretical Study of Spin States in Ni-S-4 Complexes and Models of the [NiFe] Hydrogenase Active Site. *JBIC, J. Biol. Inorg. Chem.* **2004**, *9*, 873.
(41) Dong, G.; Phung, Q. M.; Hallaert, S. D.; Pierloot, K.; Ryde, U. H2 binding to the active site of [NiFe] hydrogenase studied by multiconfigurational and coupled-cluster methods. *Phys. Chem. Chem. Phys.* **2017**, *19*, 10590.
(42) Dong, G.; Phung, Q. M.; Pierloot, K.; Ryde, U. Reaction Mechanism of [NiFe] Hydrogenase Studied by Computational Methods. *Inorg. Chem.* **2018**, *57*, 15289.
(43) Perdew, J. P. Density-functional approximation for the correlation energy of the inhomogeneous electron gas. *Phys. Rev. B: Condens. Matter Mater. Phys.* **1986**, *33*, 8822.
(44) Becke, A. D. Density-functional exchange-energy approximation with correct asymptotic behavior. *Phys. Rev. A: At., Mol., Opt. Phys.* **1988**, *38*, 3098.
(45) Tantirungrotechai, Y.; Roddecha, S.; Punyain, K.; Toochinda, P. Assessment of mixed basis set and ONIOM methods on the activation energy of ring opening reactions of substituted cyclobutenes. *J. Mol. Struct.: THEOCHEM* **2009**, *893*, 98.
(46) Weigend, F.; Ahlrichs, R. Balanced basis sets of split valence, triple zeta valence and quadruple zeta valence quality for H to Rn: Design and assessment of accuracy. *Phys. Chem. Chem. Phys.* **2005**, *7*, 3297.
(47) Peng, C.; Ayala, P. Y.; Schlegel, H. B.; Frisch, M. J. Using redundant internal coordinates to optimize equilibrium geometries and transition states. *J. Comput. Chem.* **1996**, *17*, 49.
(48) Gonzalez, C.; Schlegel, H. B. Reaction path following in mass-weighted internal coordinates. *J. Phys. Chem.* **1990**, *94*, 5523.
(49) Grimme, S.; Antony, J.; Ehrlich, S.; Krieg, H. A consistent and accurate ab initio parametrization of density functional dispersion correction (DFT-D) for the 94 elements H-Pu. *J. Chem. Phys.* **2010**, *132*, 154104.
(50) Frisch, M. J.; Trucks, G. W.; Schlegel, H. B.; Scuseria, G. E.; Robb, M. A.; Cheeseman, J. R.; Scalmani, G.; Barone, V.; Mennucci, B.; Petersson, G. A.; Nakatsuji, H.; Caricato, M.; Li, X.; Hratchian, H. P.; Izmaylov, A. F.; Bloino, J.; Zheng, G.; Sonnenberg, J. L.; Hada, M.; Ehara, M.; Toyota, K.; Fukuda, R.; Hasegawa, J.; Ishida, M.; Nakajima, T.; Honda, Y.; Kitao, O.; Nakai, H.; Vreven, T.; Montgomery, J. A., Jr.; Peralta, J. E.; Ogliaro, F.; Bearpark, M.; Heyd, J. J.; Brothers, E.; Kudin, K. N.; Staroverov, V. N.; Kobayashi, R.; Normand, J.; Raghavachari, K.; Rendell, A.; Burant, J. C.; Iyengar, S. S.; Tomasi, J.; Cossi, M.; Rega, N.; Millam, N. J.; Klene, M.; Knox, J. E.; Cross, J. B.; Bakken, V.; Adamo, C.; Jaramillo, J.; Gomperts, R.; Stratmann, R. E.; Yazyev, O.; Austin, A. J.; Cammi, R.; Pomelli, C.; Ochterski, J. W.; Martin, R. L.; Morokuma, K.; Zakrzewski, V. G.; Voth, G. A.; Salvador, P.; Dannenberg, J. J.; Dapprich, S.; Daniels, A. D.; Farkas, Ö.; Foresman, J. B.; Ortiz, J. V.; Cioslowski, J.; Fox, D. J. *Gaussian09* (revision D.01); Gaussian, Inc.: Wallingford, CT, 2009.
(51) Pounds, A. J. Valency and Bonding: A Natural Bond Orbital Donor−Acceptor Perspective. *J. Chem. Educ.* **2007**, *84*, 43.
(52) Glendening, E. D. B. J. K.; Reed, A. E.; Carpenter, J. E.; Bohmann, J. A.; Morales, C. M.; Landis, C. R.; Weinhold, F. *NBO 6.0, Theoretical Chemistry Institute*; University of Wisconsin: Madison, WI, USA, 2013.
(53) Ogata, H.; Lubitz, W.; Higuchi, Y. [NiFe] hydrogenases: structural and spectroscopic studies of the reaction mechanism. *Dalton Trans.* **2009**, *37*, 7577.
(54) Kaur-Ghumaan, S.; Stein, M. [NiFe] hydrogenases: how close do structural and functional mimics approach the active site? *Dalton Trans.* **2014**, *43*, 9392.
(55) Yagi, T.; Higuchi, Y. Studies on hydrogenase. *Proc. Jpn. Acad., Ser. B* **2013**, *89*, 16.
(56) Kampa, M.; Lubitz, W.; van Gastel, M.; Neese, F. Computational study of the electronic structure and magnetic properties of the Ni-C state in [NiFe] hydrogenases including the second coordination sphere. *JBIC, J. Biol. Inorg. Chem.* **2012**, *17*, 1269.
(57) Pearson, R. G. The electronic chemical potential and chemical hardness. *J. Mol. Struct.: THEOCHEM* **1992**, *255*, 261.
(58) Qiu, S.; Azofra, L. M.; MacFarlane, D. R.; Sun, C. Hydrogen bonding effect between active site and protein environment on catalysis performance in H2-producing [NiFe] hydrogenases. *Phys. Chem. Chem. Phys.* **2018**, *20*, 6735.
(59) Liebgott, P.-P.; Leroux, F.; Burlat, B.; Dementin, S.; Baffert, C.; Lautier, T.; Fourmond, V.; Ceccaldi, P.; Cavazza, C.; Meynial-Salles, I.; Soucaille, P.; Fontecilla-Camps, J. C.; Guigliarelli, B.; Bertrand, P.; Rousset, M.; Léger, C. Relating diffusion along the substrate tunnel and oxygen sensitivity in hydrogenase. *Nat. Chem. Biol.* **2010**, *6*, 63.

DOI: 10.1021/acs.inorgchem.8b02812
Inorg. Chem. 2019, 58, 2979−2986